Soil Dynamics and Earthquake Engineering 31 (2011) 91–103

Contents lists available at ScienceDirect

Soil Dynamics and Earthquake Engineering

journal homepage: www.elsevier.com/locate/soildyn

Experimental estimation of soil profiles through spatial phases analysis of surface waves

Marcelo A. Ceballos *, Carlos A. Prato

Department of Structures, National University of Córdoba, Av. Vélez Sarsfield 1611, X5016GCA Córdoba, Argentina

ARTICLE INFO

Article history:
Received 20 December 2008
Received in revised form
1 June 2010
Accepted 22 August 2010

ABSTRACT

The proposed techniques in recent years for the analysis of superficial waves with multiple transducers have been focused in the identification of different types of waves in the ground. The multistation tests avoid the ambiguous phase unwrapping procedure required to obtain experimental dispersion curves for the SASW technique. However, the soil profiles with stiffness inversion in depth involve the contribution of higher modes, and the inversion process through "apparent" or "effective" dispersion curves presents difficulties since these contributions depend of the transducers layout. The technique proposed herein is based on the test simulation through an updating model with low computational cost and good accuracy that include all propagation modes. Two actual test cases performed with only six transducers shows the advantages of a new objective function called "spatial phase dispersion" whose experimental determination does not require subjective interventions by the analyst.

1. Introduction

The SASW technique described by Stokoe et al. [1] has found extensive practical application for mechanical characterization of soil profiles given that it does not require boreholes since both the excitation and the recordings of wave passage are performed at the free surface. Fitting of the shear wave velocities, and eventually of the thickness of homogeneous horizontal strata with known (or assumed) density and Poisson coefficient is carried out minimizing the difference between the analytical dispersion curve and its experimental counterpart. The dispersion curves with SASW method are normally obtained assuming the ground surface motions with a highly dominant contribution of the fundamental mode of Rayleigh waves. This hypothesis is adequate in soil profiles with increasing stiffness in depth; however, the significant influence of the higher modes on the dispersion curves when the upper layers have higher stiffness, typical of pavement structures, requires that higher propagation modes be considered in the interpretation of the test results. Lai et al. [2] use the SASW technique for simultaneous adjustment of dispersion and attenuation curves to obtain the stiffness and damping properties of the soil profile. With such approach, the obtained results for profiles with growing stiffness in depth are satisfactory, although there remains the same problems associated to the multiple mode contributions.

Tokimatsu et al. [3] describe the influence of multiple propagation modes on dispersion curves. An adequate offset of the transducers referred by various authors as "filtering criteria" (for example [4]) allows to reduce the influence of higher superficial modes and body waves that become more relevant close to the point of the applied load. In fact, the contribution of different waves patterns produces an "apparent" or "effective" dispersion curve that depends of the transducers offset. The difficulty in some cases to obtain a unique dispersion curve that represents the experimental data restricts the success of the inversion process to consider the transducers layout for the superposition of different modes [5]. In this sense, Zywicki [6] obtains apparent dispersion and attenuation curves observing that partial derivatives of the adjustment parameters become unstable due to "mode jumping" effects.

Zomorodian and Hunaidi [7] propose to identify the predominant propagation mode at each frequency in function of the wave number that presents the maximum vertical flexibility coefficient. The dispersion data from different spacing are overlapped over wide frequency ranges, and for each frequency several dispersion data may be available. The dispersion data must be combined to generate the average dispersion curve (data reduction). Due to the potential dependence of the dispersion curve respect to the transducers layout, these authors propose to use a filtering criterion through which the data points at the same frequency but obtained from two different receiver spacings will be rejected if they do not match each other. In this manner, inconsistencies that might result in convergence problems during the inverse process due to multi-mode propagation are avoided.

The multichannel analysis of surface waves (MASW) proposed by Park et al. [8] increases the data redundancy, thus reducing the

* Corresponding author. Tel./fax: +54 351 4334144.
E-mail addresses: mceballo@efn.uncor.edu, chelo_ceballos@hotmail.com (M.A. Ceballos), cprato@efn.uncor.edu (C.A. Prato).

0267-7261/$ - see front matter © 2010 Elsevier Ltd. All rights reserved.
doi:10.1016/j.soildyn.2010.08.008

influence of the experimental noise and mitigating the higher superficial modes and body waves effects in the construction of smoothed versions of effective dispersion curves. Obtaining experimental dispersion curves with multiple transducers avoids the need of phase unwrapping procedures that require subjective interventions by the analyst. Yoon [9] extends the filtering criteria for multiple transducers to reduce the near-field effects and develops a procedure combining active and passive surface wave measurements. Foti [10] finds stronger inversion process utilizing multistation tests during the simultaneous adjustment of dispersion and attenuation curves. Roma [11] uses similar techniques in inversely dispersive profiles noticing the importance of considering the transducer layout in the model.

The utilization of multiple transducers has also served to develop techniques focused on the separation of different patterns of superficial waves. Zhang et al. [12] use multiple transducers for the identification of dispersion curves related with the fundamental mode although such approach can lead to difficulties when its contribution is not dominant and it is only secondary. Strobbia [13] combines probabilistic models and global search procedures to isolate the Rayleigh modes through transformations to f–k domain. Xia et al. [14] stabilize the inversion process and improve the resolution of the velocity profiles simultaneously inverting the fundamental mode and upper modes.

Some authors agree over the convenience to simulate the response at the location of the transducers considering the contribution of all modes. The use of the complete modal model of soil profiles is not new although few researchers continue to use this approach due to the high computational cost to reproduce the test results. Ganji et al. [15] propose a 3D simulation of SASW tests to involve all wave types during the inversion process of the dispersion curve. However, the analytical dispersion curve is obtained of the same form than the experimental one presenting the same lack of uniqueness and mode jumping problems. The main drawback of the simulation approach is that the exact models are computationally costly while the approximate models are not sufficiently exacts. On the other hand, the "target functions" used for the inversion process do not take advantage of all experimental information, neither have adequate sensitivity with respect to the adjustment parameters. Ryden et al. [16] propose to use multimodal dispersion curves as target in the analysis of pavement structural systems. Ryden et al. [17] carry out the inversion process with the complete spectrum of the phase velocities, thus avoiding the often difficult modes separation. The target function they use is a nondimensional version of the phase-velocity spectra proposed by Park et al. [18,19], although it requires a high number of transducers for a satisfactory resolution. The problem of convergence to local minima is resolved using global search procedures based on the inversion technique of fast simulated annealing.

The technique proposed in the present work considers all propagation modes during the adjustment through a variation of the "thin layers formulation" [20,21] that leads to good accuracy and low computational cost. A relatively small number of transducers allows the definition of a target function, here designated as "spatial phase dispersion", that produces an efficient reduction of the experimental data. This function, originally defined in the frequency domain with the name of phase dispersion [22], is now used in the wave number domain. The determination of the spatial phase dispersion does not require the intervention of the analyst, as is normally done in the unwrapping procedure of the spectral phase for obtaining of dispersion curves. This is possible because the values for each frequency do not depend on adjacent frequencies' values. The spatial phase dispersion represents a surface whose ordinates vary between 0 and 1 independently of the number of transducers; the two independent variables are the period of excitation of the source and the propagation velocity of surface waves. The excitation period is used instead of the frequency because the discretization of this variable with fixed increments produces a better distribution of the experimental information. The surface presents minimum values or "valleys" in correspondence with the dominant propagation velocities for each excitation period. These minima are related to the effective dispersion curve of the SASW technique. The spurious valleys that appear in this surface due to the spatial aliasing can be distinguished easily of the main valley considering the spatial discretization parameters.

A least square minimization of the difference between the experimental and analytical phase dispersion allows parameter adjustment of different strata of the soil profile even in cases of soft strata underlying hard strata. The variability of the group velocity with offset and number of transducers is explicitly considered, turning out to be unnecessary to construct a unique curve valid for all the experimental data, as is the case in the SASW technique. Although this work does not deal with the problem of convergence to local minima, the new target function can be incorporated in algorithms as the proposed by Degrande et al. [23].

2. Soil profile model

The analytical model used in the inversion process is based on the "thin layers formulation" [20,21] with a variation for the halfspace model that supports the strata of the soil profile. This formulation is usually adopted in obtaining the dispersion curves given that it allows the response modal decomposition with low computational cost. However, the approximation adopted for the halfspace only provides good accuracy for the fundamental mode. The approximation of the components of the exact stiffness matrices of halfspace through polynomial fractions using experimental modal analysis techniques accurately represents the higher modes and at the same time preserves the computational advantages of this formulation.

2.1. Stiffness matrices for layered soils

The exact matrices of the response in the wave number domain k in the interface among horizontal strata are presented in works of Kausel [20] and Kausel and Roësset [21]. The Hankel transform that allows to convert the response from wave number domain k to the spatial domain ρ requires numerical implementations that turn out to be computationally costly. The thin layers formulation proposed by the same authors expands the transcendental functions in k of the exact matrix coefficients in quadratic polynomial of k:

$$K = Ak^2 + Bk + C, \tag{1}$$

where $C = G - \omega^2 M$, and ω represents the excitation frequency in rad/sec. The global matrix K of the soil profile is then built through the assemblage of the elementary matrices of L strata that link the generic interfaces 1 and 2 satisfying the following equilibrium equation:

$$\begin{Bmatrix} K_{xx}^{11} & K_{xz}^{11} & K_{xx}^{12} & K_{xz}^{12} \\ K_{zx}^{11} & K_{zz}^{11} & K_{zx}^{12} & K_{zz}^{12} \\ K_{xx}^{21} & K_{xz}^{21} & K_{xx}^{22} & K_{xz}^{22} \\ K_{zx}^{21} & K_{zz}^{21} & K_{zx}^{22} & K_{zz}^{22} \end{Bmatrix} \begin{Bmatrix} U_x^1 \\ U_z^1 \\ U_x^2 \\ U_z^2 \end{Bmatrix} = \begin{Bmatrix} P_x^1 \\ P_z^1 \\ P_x^2 \\ P_z^2 \end{Bmatrix}, \tag{2}$$

where x represents the radial coordinate and z represents the vertical coordinate. The response in a vertical plane in k domain is

obtained as

$$KU = P \Longrightarrow U = K^{-1}P = FP. \tag{3}$$

The resolution of the eigenvalues problem of the complete system:

$$(Ak_l^2 + Bk_l + C)\Phi_l = 0, \tag{4}$$

allows to express the spatial response through the superposition of all propagation modes in closed form avoiding the explicit application of Hankel transform. The vertical displacement in the surface U_z in wave number domain k and in spatial domain ρ results

$$U_z(k) = \sum_{l=1}^{2L} \frac{\Phi_{z,l}^2}{(k^2 - k_l^2)} \iff U_z(\rho) = \frac{1}{4i} \sum_{l=1}^{2L} \Phi_{z,l}^2 \, H_0^{(2)}(k_l \rho), \tag{5}$$

where L is the strata number, k_l represents the eigenvalues, $\Phi_{z,l}$ represents the vertical component of the eigenvectors in the surface, and $H_0^{(2)}(\cdots)$ is the second function of Hankel of order 0. The matrices of the thin layers formulation present good accuracy for small thicknesses with respect to wave length λ; otherwise, the layers can be subdivided into sublayers until reaching the desired accuracy. An adequate discretization of soil layers depends on the shear wave velocity of the stratum V_S and should satisfy the following condition:

$$\Delta h \leq \lambda/10 \tag{6a}$$

$$\leq V_S/(10\, f), \tag{6b}$$

where f represents the excitation frequency in Hz. The value 1/10 empirically adopted in Eq. (6) represents a conservative value with respect to values 1/5–1/8 usually adopted for finite element models of soil–structure systems. This value allows a greater precision than accepted for the dynamic response of these systems without an appreciable increment of computational cost.

The applied load on the ground surface during the experimental tests is assumed here to be a vertical point load. The analytical solution of the response (Pekeris's problem) presented by Kausel [24] allows to check numerical solutions obtained with approximate matrices used for the homogeneous halfspace model. The input load is described in the k and ρ domains as

$$P_z(k) = 1 \iff P_z(\rho) = \delta(\rho)/\rho, \tag{7}$$

where $\delta(\cdots)$ represent the Dirac delta function. The vertical response in k domain is according to (3) numerically equal to the first vertical component of the flexibility matrix main diagonal.

2.2. Approximate matrices for homogeneous halfspace

The halfspace model originally proposed for the thin layers formulation relies on 8–10 strata with increasing thickness in depth covering 1.5 times the wave length of the propagation fundamental mode where the maximum displacements are produced. This strategy allows to obtain adequate precision to the fundamental mode used to construct the analytical dispersion curve of SASW technique. Nevertheless, the strategy generates spurious modes that distort the response in spatial domain more severely to greater distances of the input load. Fig. 1 shows a comparison of normalized coefficients of approximate and exact flexibility versus normalized wave number for horizontal (left) and vertical (right) displacements. Note that fundamental mode has the highest wave number and approximate coefficients possess null imaginary part.

The approximation proposed in this work consists to use halfspace matrices with the same mathematical structure of thin layer matrices to continue avoiding the explicit application of the computationally costly Hankel transform. The approximation of dynamic flexibilities with polynomial fractions is exhaustively utilized in experimental modal analysis [25] and is also used to reproduce complex analytical solutions [26]. The works of Ceballos et al. [27] and Ceballos [28] present several cases where the response of soil-structure interaction systems is approached through experimental modal analysis techniques.

The application of these adjustment techniques has allowed to obtain discrete matrices as those given in Appendix A that accurately reproduce the dynamic flexibility curves of the halfspace as can be observed in Fig. 2. A hysteretic damping $\beta = 0.005$ is assumed to the soil. The adjustment process begins with the halfspace modeled through 5 strata with increasing thickness in depth. The modal parameters extracted of these halfspace global matrices are then adjusted through small steps of iteration until convergence. The normalized results allow to use the adjusted matrices for different values of the shear wave velocities; the optimization procedure should be repeated for different values of Poisson coefficient, and eventually for different values of hysteretic damping. These matrices may be included in a database during the adjustment procedure.

The modal shape components cannot take arbitrary values since that would break the special structure of the strata matrices

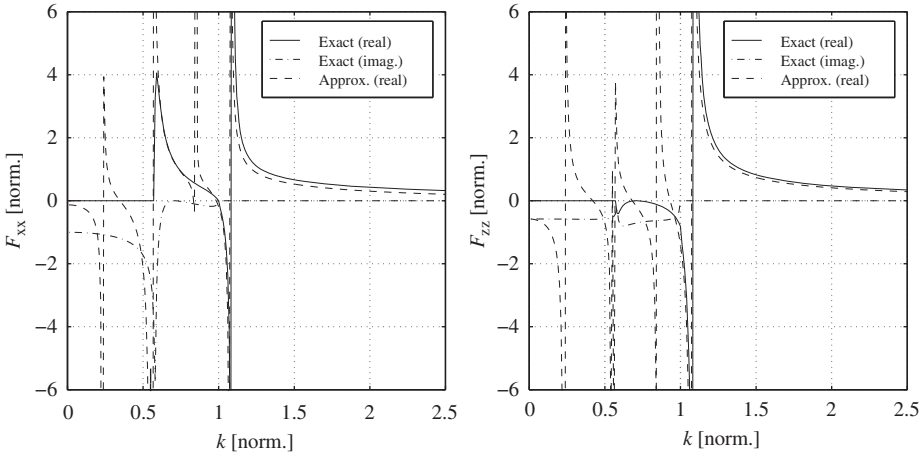

Fig. 1. Original approximate flexibility of homogeneous halfspace ($v = 0.25$).

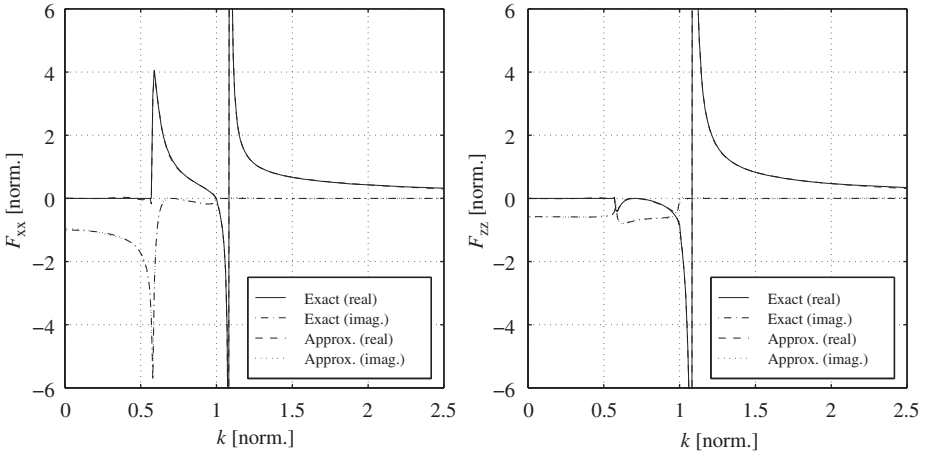

Fig. 2. Improved approximate flexibility of homogeneous halfspace ($v = 0.25$).

[20]. Therefore, the optimization procedure incorporates restrictions to the modal shapes to maintain this structure allowing to pass from k domain to ρ domain in analytical form. These restrictions should also be satisfied for complex modal shapes of mechanical systems with non-classical damping whose movement equations are expressed in state space formulation. Garvey et al. [29,30] present detailed studies of this type of systems that require to satisfy the called "fundamental restriction".

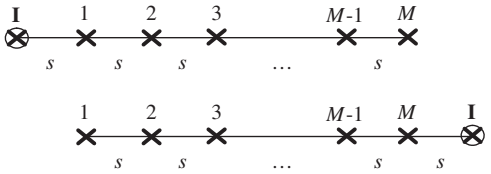

Fig. 3. Transducers layout on ground surface.

3. Spatial phase dispersion

The adjustment of shear wave velocities of different strata is carried out through a least square minimization of the difference between experimental and analytical versions of the spatial phase dispersion. This function depends on offset and number of transducers. Fig. 3 shows the suggested layout for M uniaxial sensors placed in a vertical direction on the ground surface. The s parameter represents the transducers offset among themselves just like the distance between input load and first transducer. This parameter is duplicated after the execution of 5–10 impacts in each end of the transducers line.

At this point, it may be pointed out that the main advantages to take records of the ground movement only in a vertical direction are: (a) the vertical amplitudes are usually greater than the horizontal ones having better signal-to-noise relation; (b) a greater number of measurement points over the ground for the same number of channels, and (c) the relation between vertical and horizontal ground movement components that would be used for the model updating may be affected by material damping.

3.1. Analytical definition

The purpose of the spatial phase dispersion is to quantify for each frequency the continuity of spatially discretized surface waves for a given position of the transducers by means of different "testing-phase velocities" (according to the terminology used by Ryden and Park [17]). The analytical form of the spatial phase dispersion is constructed with the relative spatial phase among transducers as follows:

(1) To quantify the continuity of the surface waves, the spectral response for each excitation frequency (or period) ω_i of each transducer m is "synchronized" as a function of the distance to the input load ρ_m and of the testing-phase velocity V_j by dividing the spectral response U_{im} by the Hankel function $H_0^{(2)}(\cdots)$:

$$\overline{U}_{ijm} = \frac{U_{im}}{H_0^{(2)}(\omega_i/V_j \cdot \rho_m)}. \tag{8}$$

This type of synchronization is designated by Zywicki [6] as a cylindrical beamforming equation. However, the target function obtained in their approach after the combination of the records of different transducers turns out to be essentially different with respect to the spatial phase dispersion.

(2) The relative spatial phase of each transducer m for each excitation frequency ω_i and testing-phase velocity V_j is equal to the complex amplitude angle:

$$\varphi_{ijm} = \text{angle}(\overline{U}_{ijm}). \tag{9}$$

(3) The spatial phase dispersion Γ_{ij} of frequency ω_i and velocity V_j is obtained by relating the relative spatial phase of the M transducers among themselves:

$$\Gamma_{ij} = \sum_{m=1}^{M-1} \sum_{n=m+1}^{M} \frac{\begin{pmatrix} (\sin\varphi_{ijm} - \sin\varphi_{ijn})^2 + \cdots \\ (\cos\varphi_{ijm} - \cos\varphi_{ijn})^2 \end{pmatrix}}{M^2}, \quad n > m. \tag{10}$$

The basis for this expression is the fact that a single surface wave propagating at frequency ω_i at a propagation velocity V_j is such that all terms under the summation sign are cancelled due to the synchronization of the spatial phase. In general, the terms under the summation sign tend to grow when the velocity departs from the dominant values of the propagation velocities. The factor M^2 leads to the condition that the maximum value of the phase dispersion has unity as an upper bound.

It is worth pointing out that the spatial phase dispersion, used as a target function in the inversion process, may be interpreted as a surface defined in terms of two independent variables

(frequency – or period – of the excitation, and the testing-phase velocity) which is only valid for a given number and spatial distribution of the transducers. As a consequence of this, the adjustment between experimental and analytical spatial phase dispersions corresponding to different transducer layouts are to be adjusted separately.

Alternative expressions for the spatial phase dispersion mathematically identical to (10) are obtained in terms of the synchronized spectral amplitudes:

$$\Gamma_{ij}=\frac{1}{M^2}\sum_{m=1}^{M-1}\sum_{n=m+1}^{M}\begin{pmatrix}\left(\dfrac{\overline{U}_{ijm}}{|\overline{U}_{ijm}|}-\dfrac{\overline{U}_{ijn}}{|\overline{U}_{ijn}|}\right)\bullet\cdots\\ \left(\dfrac{\overline{U}^*_{ijm}}{|\overline{U}_{ijm}|}-\dfrac{\overline{U}^*_{ijn}}{|\overline{U}_{ijn}|}\right)\end{pmatrix}, \tag{11}$$

$$\Gamma_{ij}=\frac{1}{M^2}\sum_{m=1}^{M-1}\sum_{n=m+1}^{M}\begin{pmatrix}\dfrac{\overline{U}_{ijm}|\overline{U}_{ijn}|-\overline{U}_{ijn}|\overline{U}_{ijm}|}{|\overline{U}_{ijm}||\overline{U}_{ijn}|}\bullet\cdots\\ \dfrac{\overline{U}^*_{ijm}|\overline{U}_{ijn}|-\overline{U}^*_{ijn}|\overline{U}_{ijm}|}{|\overline{U}_{ijm}||\overline{U}_{ijn}|}\end{pmatrix}, \tag{12}$$

$$\Gamma_{ij}=\frac{1}{M^2}\sum_{m=1}^{M-1}\sum_{n=m+1}^{M}\left(2-\frac{\overline{U}_{ijm}\overline{U}^*_{ijn}+\overline{U}_{ijn}\overline{U}^*_{ijm}}{|\overline{U}_{ijm}||\overline{U}_{ijn}|}\right), \tag{13}$$

$$\Gamma_{ij}=\frac{1}{M^2}\sum_{m=1}^{M-1}\sum_{n=m+1}^{M}\left(2-\frac{\overline{U}_{ijm}\overline{U}^*_{ijn}+\overline{U}_{ijn}\overline{U}^*_{ijm}}{\sqrt{\overline{U}_{ijm}\overline{U}^*_{ijm}\overline{U}_{ijn}\overline{U}^*_{ijn}}}\right). \tag{14}$$

The last equation leads to a more convenient form for the experimental data since it involves spectral densities S_{ijmn} (defined further on in the paper) that they allow the possibility of averaging records from different experiments or runs in order to reduce the influence of random noise:

$$\Gamma_{ij}=\frac{1}{M^2}\sum_{m=1}^{M-1}\sum_{n=m+1}^{M}\left(2-\frac{S_{ijmn}+S_{ijnm}}{\sqrt{S_{ijmm}S_{ijnn}}}\right). \tag{15}$$

Separating the summation from the constant term one arrives at

$$\Gamma_{ij}=1-\frac{1}{M}-\frac{1}{M^2}\sum_{m=1}^{M-1}\sum_{n=m+1}^{M}\frac{S_{ijmn}+S_{ijnm}}{\sqrt{S_{ijmm}S_{ijnn}}}. \tag{16}$$

An alternative target function that could be used to adjust the soil profile with identical results, which is closely related to the normalized phase-velocity spectra proposed by Ryden and Park [17], consists of the spatial phase coherence defined as follows:

$$\Psi_{ij}=1-\Gamma_{ij}=\frac{1}{M}+\frac{1}{M^2}\sum_{m=1}^{M-1}\sum_{n=m+1}^{M}\frac{S_{ijmn}+S_{ijnm}}{\sqrt{S_{ijmm}S_{ijnn}}}. \tag{17}$$

In this case, a value of Ψ_{ij} close to unity would indicate a high spatial coherence of the surface waves for the excitation frequency ω_i and the propagation velocity V_j.

The synchronization of spectral phase in Eq. (8) could be carried out through a complex exponential (assuming a 2D waves propagation model) as

$$\overline{U}_{ijm}=\frac{U_{im}}{\exp(I\omega_i/V_j\cdot\rho_m)}. \tag{18}$$

However, the Hankel function better represents the 3D propagation especially near of the input load. In fact, the analytical solution of the vertical displacement on a homogeneous halfspace presented by Lamb [31] results in

$$U_z(k)=\frac{\Phi_R^2}{(k^2-k_R^2)}\iff U_z(\rho)=\frac{1}{4i}\Phi_R^2\,H_0^{(2)}(k_R\rho), \tag{19}$$

with

$$\Phi_R^2=\frac{1}{G}\frac{k_S^2(k_R^2-k_P^2)\sqrt{k_R^2-k_S^2}}{\left(8k_R^4-6k_R^2(k_P^2+k_S^2)+4k_P^2k_S^2+(4k_S^2-8k_R^2)\sqrt{k_R^2-k_P^2}\sqrt{k_R^2-k_S^2}\right)}. \tag{20}$$

$$G=\delta V_S^2,\quad k_P=\omega/V_P,$$

$$k_S=\omega/V_S,\quad k_R=\omega/V_R, \tag{21}$$

where δ is the halfspace density, and V_P, V_S and V_R are propagation velocities of P, S and Rayleigh waves, respectively.

A convenient representation of the spatial phase dispersion is obtained through contour lines as a function of the excitation period and of the propagation velocity. The three profiles described in Table 1 are studied in order to show the general aspect of this function. Case I represents a stratum of 4 m thickness with $V_S = 200$ m/s over a homogeneous halfspace with $V_S = 400$ m/s. Case II considers a stratum of 4 m thickness with $V_S = 400$ m/s over a homogeneous halfspace with $V_S = 200$ m/s. Case III represents a stratum of 4 m thickness with $V_S = 200$ m/s over another stratum of 4 m thickness with $V_S = 400$ m/s, and a lower homogeneous halfspace with $V_S = 200$ m/s. All cases adopt a density $\delta = 2.0\,\mathrm{tn/m^3}$ and a Poisson coefficient $\nu = 1/3$.

Figs. 4–6 present the spatial phase dispersion obtained using eight transducers with different offsets for cases described in Table 1. The dependence of the dominant propagation velocity with transducers offset is clearly observed in these figures (thick continuous line). The zone above the dash lines represents wave lengths greater than the distance between the impact point and the last transducer ($\lambda > \lambda_{\max}$). The zone below the dash-dot lines represents wave lengths with deficient sampling rate that would be affected by aliasing effects ($\lambda < \lambda_{\min}$): observe minimum spatial phase dispersion strips not related with dominant propagation velocities. The zone of recommended values for the adjustment is found between both described lines (shaded zone). The position of these boundary lines depends on number and offset of transducers according to the following expressions:

$$\left.\begin{aligned}&\lambda_{\max}=V_{\max}T=Ms\Rightarrow V_{\max}=Ms/T\quad\text{(dash lines)}\\&\lambda_{\min}=V_{\min}T=2s\Rightarrow V_{\min}=2s/T\quad\text{(dash}-\text{dot lines)}\end{aligned}\right\}. \tag{22}$$

3.2. Experimental determination

The experimental spatial phase dispersion is obtained from tests as follows:

(1) The spectral response for each excitation frequency (or period) ω_i, each transducer m and each test sample p is obtained through the Fourier transform as (t_q represents a

Table 1
Study cases of spatial phase dispersion.

Layer	Thickness (m)	Shear waves velocity (m/s)		
		Case I	Case II	Case III
1	4	200	400	200
2	4	–	–	400
Halfspace	∞	400	200	200

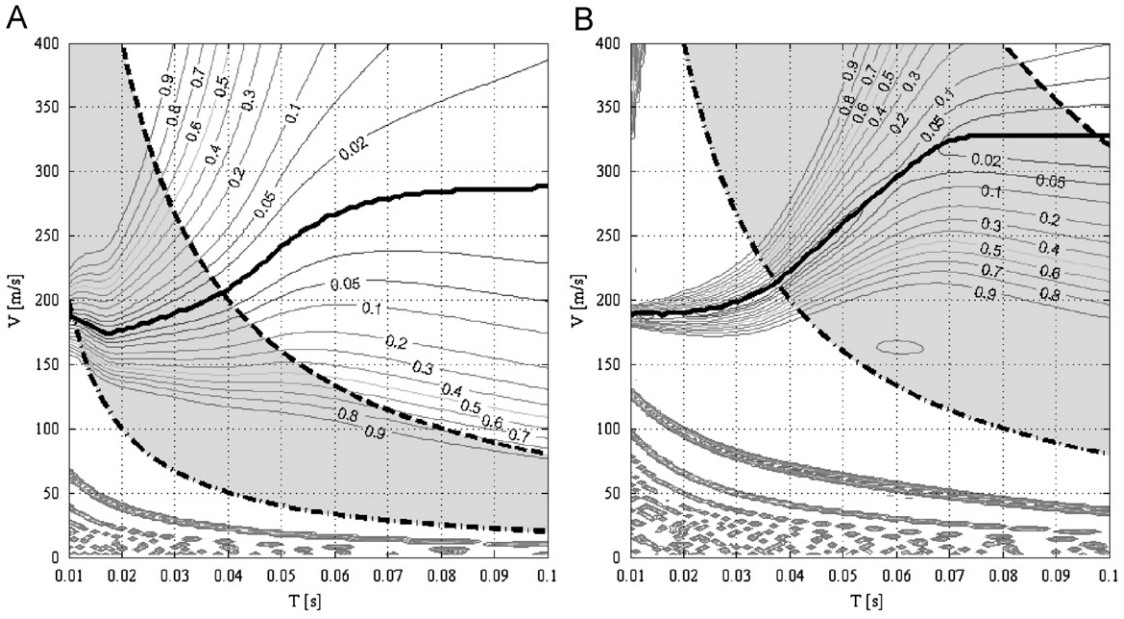

Fig. 4. Spatial phase dispersion for Case I: 8 transducers with offset of (A) 1 m and (B) 4 m.

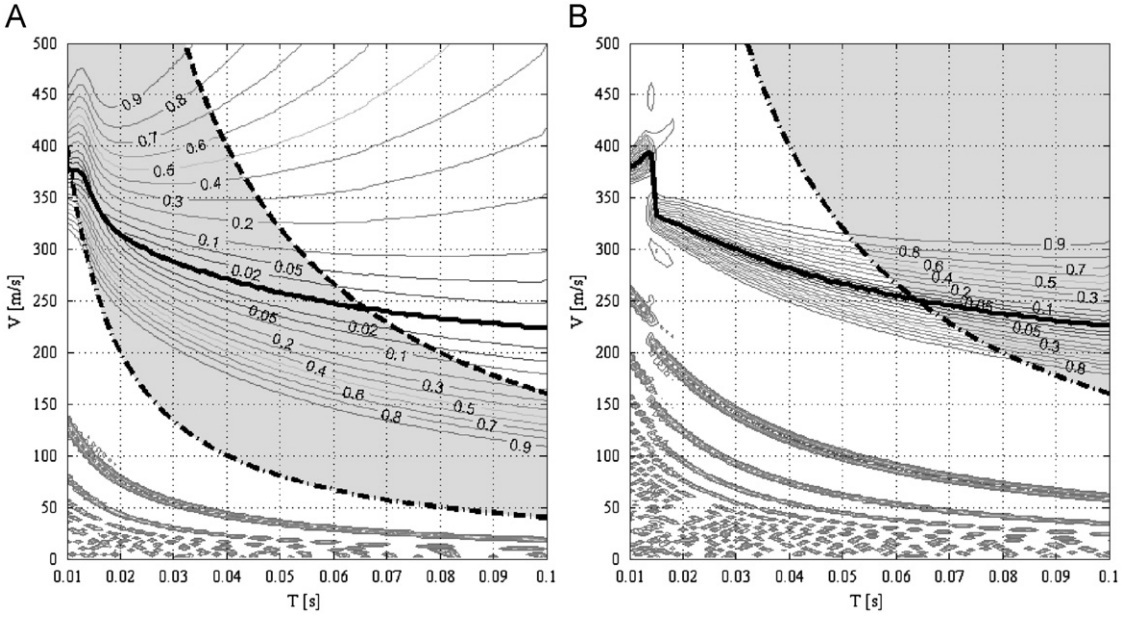

Fig. 5. Spatial phase dispersion for Case II: 8 transducers with offset of (A) 2 m and (B) 8 m.

time sample from a total of Q samples)

$$U_{imp} = \sum_{q=1}^{Q} u_{mp}(t_q)\exp(-I\omega_i t_q). \tag{23}$$

(2) The synchronized spectral response in function to input distance ρ_m and propagation velocity V_j is calculated through the Hankel function $H_0^{(2)}(\cdots)$:

$$\overline{U}_{ijmp} = \frac{U_{imp}}{H_0^{(2)}(\omega_i/V_j \cdot \rho_m)}. \tag{24}$$

(3) The spectral densities are obtained from the P test samples averaging the products of the synchronized spectral response of transducer m by the complex conjugate one of transducer n:

$$S_{ijmn} = \frac{1}{P}\sum_{p=1}^{P} \overline{U}_{ijmp}\overline{U}^{*}_{ijnp}. \tag{25}$$

(4) The spacial phase dispersion of frequency ω_i and velocity V_j is calculated through the expression (15) in function of spectral densities.

The global spectral coherence of the experimental data for definition of confidence ranges can be tentatively obtained for each excitation period T_i as the arithmetical average of the coherence of all transducers among themselves.

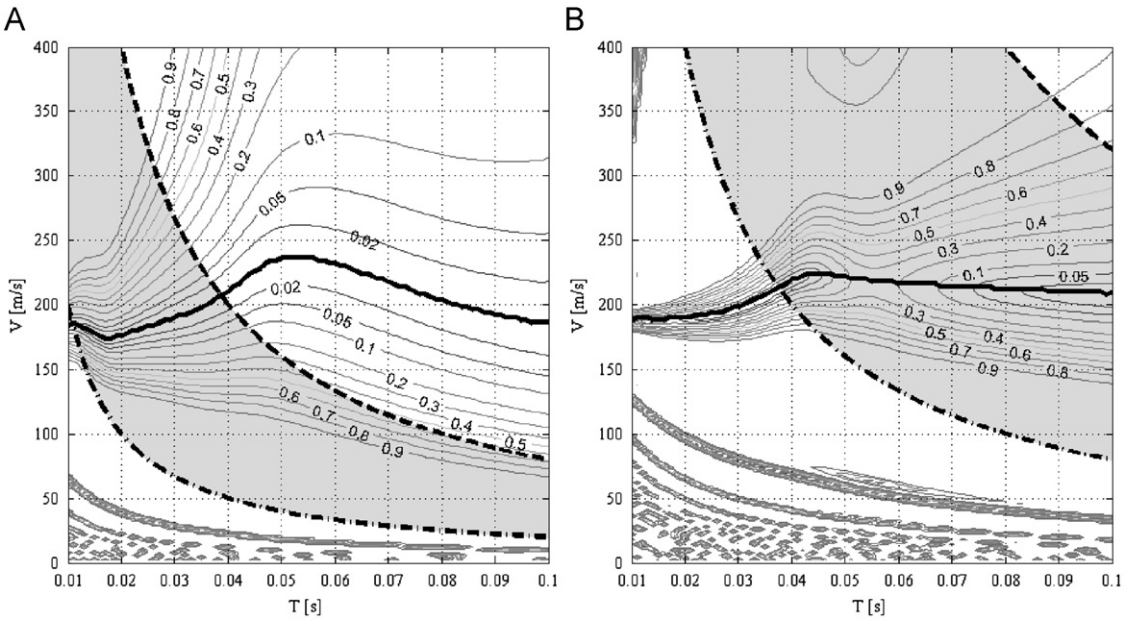

Fig. 6. Spatial phase dispersion for Case III: 8 transducers with offset of (A) 1 m and (B) 4 m.

4. Procedure of model updating

The adjustment of shear wave propagation velocities of different strata is carried out through simultaneous minimization of the difference between experimental and analytical versions of the spatial phase dispersion of each transducer layout used for the tests. The range of frequencies defined for the adjustment process depends on the depth of interest, which is naturally conditional to attaining sufficiently high coherence in that range. The adjustment velocities are defined through expressions (22) in terms of the involved wave lengths. In this way, the adjustment region of the surface representing the spatial phase is within the shaded area of Figs. 4–6.

An adequate conditioning of the updating equation system is obtained choosing as adjustment parameters the fractional change of strata velocities $\{p\}$ according to common techniques in experimental modal analysis [25]:

$$\{V_U\} = \{V_I\}(1+\{p\}), \tag{26}$$

where $\{V_U\}$ and $\{V_I\}$ are adjusted and initial shear wave velocity vectors, respectively, in each iteration step. The initial values vector of strata velocities can be defined through the raw experimental data. The experimental phase dispersion is expressed in terms of the initial value for each iteration as

$$\Gamma_{ij}^{X} = \Gamma_{ij}^{I} + \sum_{l=1}^{N_p} \frac{\partial \Gamma_{ij}^{I}}{\partial p_l} p_l. \tag{27}$$

Eq. (27) is strictly valid for small variations of updating parameters so that the maximum variation rate of the velocities for each iteration must be limited. The system to solve using the least square criterion is

$$\left\{ \frac{\partial \Gamma_{ij}^{I}}{\partial p_1} \quad \frac{\partial \Gamma_{ij}^{I}}{\partial p_2} \quad \cdots \quad \frac{\partial \Gamma_{ij}^{I}}{\partial p_{N_p}} \right\} \{p\} = \Gamma_{ij}^{X} - \Gamma_{ij}^{I}. \tag{28}$$

The root mean square of the difference between experimental and analytical versions of the spatial phase dispersion (independent term of Eq. (28)) for all transducer layouts used in the tests is utilized as error norm for convergence control during the inversion process.

The sensitivity matrix that multiplies the adjustment parameters vector $\{p\}$ is updated at each iteration evaluating the derivatives of the spatial phase dispersion through the chain rule. The spectral response used in Eq. (8) is expressed in terms of modal parameters form the eigenvalue problem of the thin layers formulation according to (5). Friswell et al. [32] present the partial derivatives of complex eigenvalues and eigenvectors of a damping system with respect to its physical parameters that are directly applicable to the layered soil model replacing the frequency ω by the wave number k.

The need of iterations during the adjustment process is due to the linearization of the components of the sensitivity matrix. It may also be convenient to set limit values to the adjustment parameters in each iteration to maintain the validity of linearized expressions.

The Poisson coefficient and hysteretic damping relations are not chosen as updating parameters due to the lack of sensitivity of the spatial phase dispersion against these parameters, as compared with shear wave velocities. Nevertheless, the repetition of the adjustment procedure with different sets of these parameters can provide an estimation of the optimum values. The spatial phase dispersion has low sensitivity with respect to velocity changes of deep strata whose values are close to the real ones, as it happens with the dispersion curves of the SASW technique.

5. Experimental studies

Two test cases are now presented in order to illustrate the main features of the proposed target function. These cases correspond to two different soil profiles that may be considered representative of typical situations near the authors base; the first one corresponds to a deep loessic formation with normally dispersive profile (increasing stiffness in depth), while the second one is a site with a pavement layer, i.e. inversely dispersive. The selection of the test cases was based on the need to gather all the experimental data with the same set of transducers and recording equipment that is required to apply the proposed procedure with

a limited logistic effort. As a consequence, the procedure is not compared with other similar approaches mentioned in the literature but rather with other readily testing techniques available to the authors.

Fig. 7. Application of impulsive load and transducers layout for Case 1.

Table 2
Fitted shear waves velocities for Case 1.

Layer	Thickness (m)	Poisson's ratio	Density (tn/m^3)	V_S (m/s)
1	1.00	1/3	1.40	217
2	1.00	1/3	1.40	220
3	1.00	1/3	1.40	222
4	1.00	1/3	1.40	220
5	1.00	1/3	1.40	220
6	1.00	1/3	1.40	217
7	1.00	1/3	1.40	222
8	1.00	1/3	1.40	211
Halfspace	∞	1/3	1.40	211

5.1. Case 1: normally dispersive profile

5.1.1. Test description

The input load on the ground surface was applied dropping a steel mass of 0.5 kN from a height of about 1.7 m from a tripod shown in Fig. 7. The layout of the six HBM accelerometers used as transducers is also given in this figure. The amplifier/conditioner (model Spider 8) used has eight input channels set with a Butterworth low-pass filter at 75 Hz. This equipment is handled through special software installed in a portable computer together with the test records. Each of the experimental signals has a duration of 2.5 sec and a sampling frequency of 600 Hz that produces 1500 points per record. The sensors were placed using four layouts on the ground with offsets of 0.5, 1, 2 and 4 m. The spectral coherence to define the rank of confident periods was obtained through five tests for each layout.

5.1.2. Analysis of results

The soil at the testing site is "loess"; according to available studies [28,33] it has an approximate density $\delta = 1.4\,\mathrm{tn/m^3}$ and a Poisson coefficient of $v = 1/3$. A preliminary analysis of the raw experimental data suggests to discretize the soil profile model in 8 strata of 1 m thickness each over a homogeneous halfspace. These strata are then divided into sublayers with the same properties depending of the analysis frequency according to Eq. (6). The initial value of shear wave velocities of the strata and halfspace is $V_S = 200$ m/s. The maximum variation rate of shear wave velocities defined for each iteration was 0.01.

Figs. 8–11 show a comparison of experimental and adjusted spatial phase dispersion surfaces for transducer offsets of 0.5, 1, 2 and 4 m, respectively. The general distribution of contour lines of analytical and experimental versions of the spatial phase dispersion present a marked similarity even in the aliasing zone below the dash-dot lines. The spectral coherence obtained as the average of values calculated for all the transducers in pairs is shown below

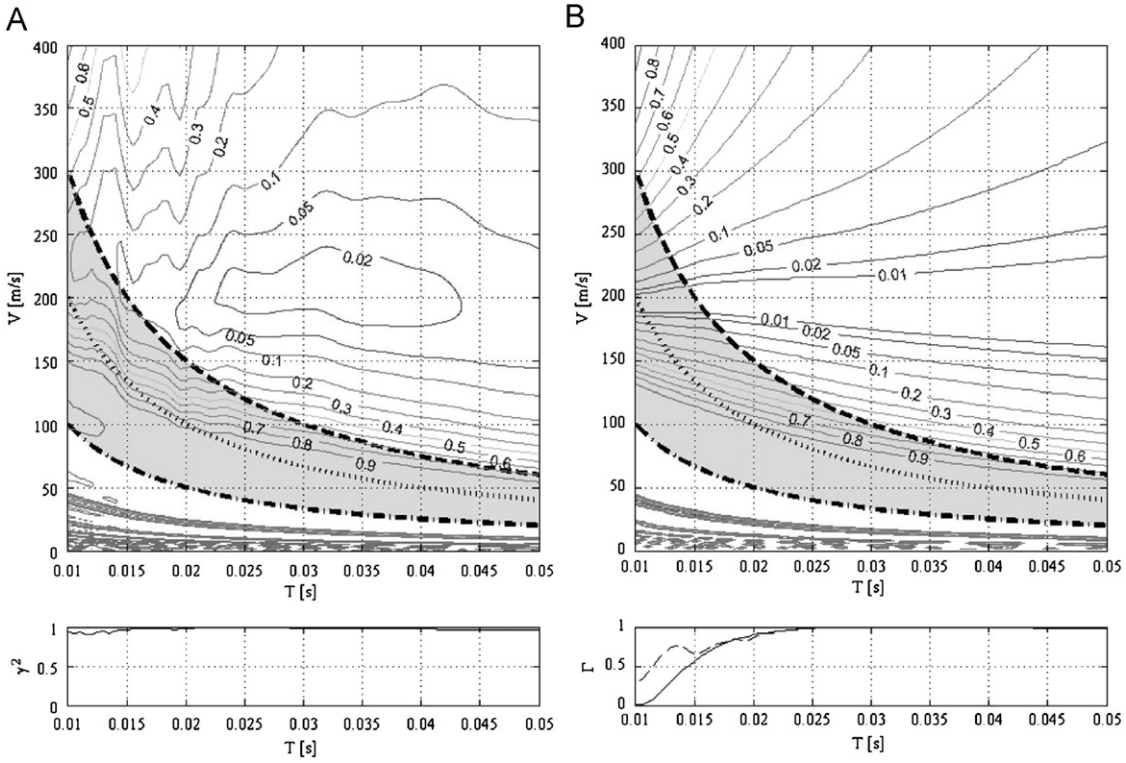

Fig. 8. Spatial phase dispersion for a transducer offset of 0.5 m: (A) Experimental and (B) Analytical.

the experimental surfaces. Their values fell for periods smaller than 0.015 sec due to the effect of the low-pass filter, while the offsets of 2 and 4 m show a marked general fall by a combined effect of smaller signal/noise relation, due to geometric attenuation of surface waves, and the use of long cables to reach the most distant transducers.

A comparison of the spatial phase dispersion as a function of the excitation period T, taking the values of the propagation velocity given by the expression $V=4s/T$ (it is marked at the center of the shaded area by a dot line) is shown below the analytical surfaces. The continuous lines represent the analytical version of the spatial phase dispersion while the dash lines

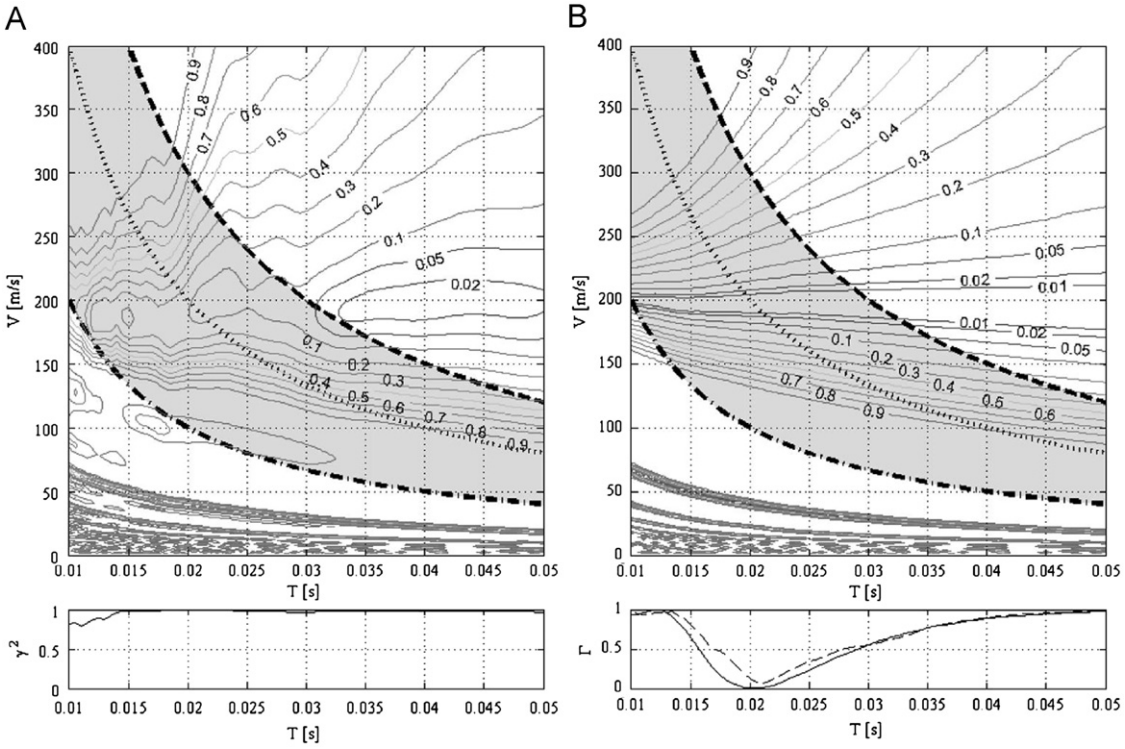

Fig. 9. Spatial phase dispersion for a transducer offset of 1 m: (A) Experimental and (B) Analytical.

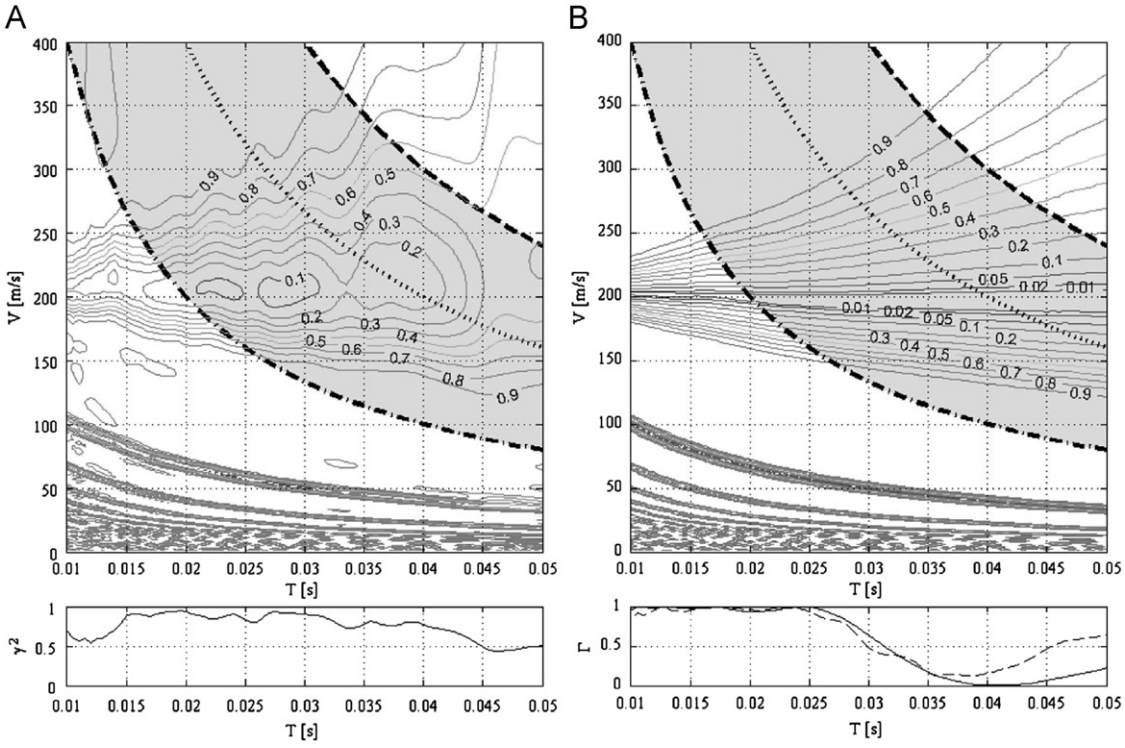

Fig. 10. Spatial phase dispersion for a transducer offset of 2 m: (A) Experimental and (B) Analytical.

represent the experimental counterpart (noting that in some cases the comparison extends beyond the adjustment region). The root mean square of the difference between analytical and experimental surfaces of the spatial phase dispersion turns out to be $\varepsilon_{\mathrm{rms}} = 0.114$.

The final adjusted values of the shear waves velocities shown in Table 2 are within the range of values measured by Rinaldi et al. [34] through bender elements in a sample obtained nearby with a moisture content $w = 15-20\%$ during an oedometric test. The SASW technique applied in the adjacent area of the test field [28] gave values of $V_S = 160-180\,\mathrm{m/s}$ near the surface, while for depths larger than 3 m values of $V_S = 190-225\,\mathrm{m/s}$ were reported. Down-hole tests performed by Rinaldi et al. [35] are in the range of $V_S = 200-320\,\mathrm{m/s}$ for depths up to 5 m. These results show that the values obtained using different experimental techniques may exhibit marked differences among them. The differences among these techniques are attributed to the extension of the soil profile covered during the tests, considering possible heterogeneousness inside each stratum, to the capacity of each technique of mitigating the experimental noises, and to the consistency between the analytical and experimental versions of the target function, among other factors.

The adjusted soil profile presents basically uniform velocities that could also have been obtained with the original SASW technique. The proposed method, however, can be fully automated and does not require subjective user interventions.

5.2. Case 2: inversely dispersive profile

5.2.1. Test description

The input load on the pavement surface was applied manually through a steel hammer with a mass of 20 N. The impact point of the hammer together with the layout of the same accelerometers used in Case 1 is given in Fig. 12. A Butterworth low-pass filter at 200 Hz was used for all channels. Each experimental record has a duration of 1.0 sec and a sampling frequency of 1200 Hz. The sensors were placed on the pavement in two different offsets: 0.30 and 0.60 m. The spectral coherence to define the rank of validity was obtained by repeating the tests five times for each transducer layout.

5.2.2. Analysis of results

The profile consists of a concrete asphalt layer with a thickness of 0.05 m over a base of granular material with a thickness of 0.10 m. Both strata rest on the same loessic formation of Case 1, that is discretized in three strata of 0.20, 0.40 and 0.80 m thickness, respectively, on a homogeneous halfspace. The initial values of shear wave velocities of the asphalt, granular base and loessic formation are 800, 400 and 200 m/s, respectively. The maximum variation rate of shear wave velocities defined for each iteration was 0.005.

Figs. 13 and 14 show a comparison of experimental and adjusted spatial phase dispersion for transducer offsets of 0.30 and 0.60 m, respectively. The contour lines of analytical and experimental spatial phase dispersion are very similar within the

Fig. 12. Application of impulsive load and transducers layout for Case 2.

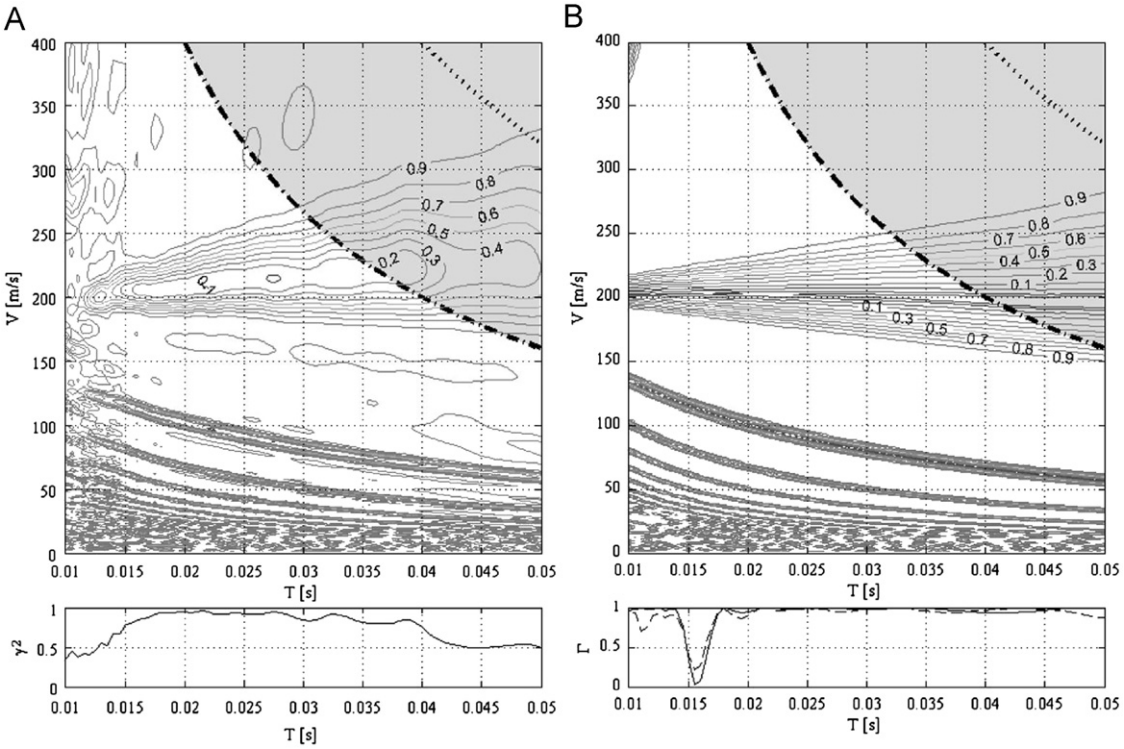

Fig. 11. Spatial phase dispersion for a transducer offset of 4 m: (A) Experimental and (B) Analytical.

shaded zone. The spectral coherence shown below the experimental surfaces presents values over 0.9 throughout the frequency range. A comparison of the spatial phase dispersion in terms of the excitation period T, for the velocities given by $V=4s/T$, is shown below the analytical surfaces. The continuous lines represent the analytical version of the spatial phase dispersion while the dashed lines represent the experimental counterpart. The root mean square of the difference between analytical and experimental surfaces of the spatial phase dispersion turns out to be $\varepsilon_{\mathrm{rms}}=0.111$.

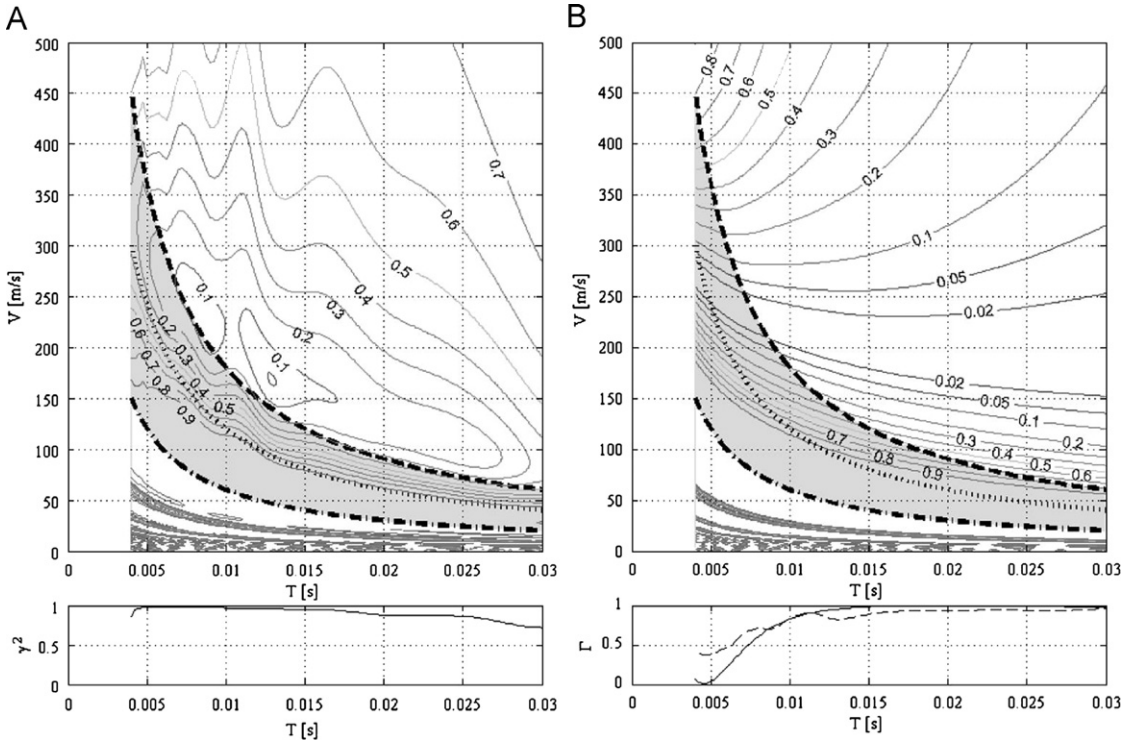

Fig. 13. Spatial phase dispersion for a transducer offset of 0.30 m: (A) Experimental and (B) Analytical.

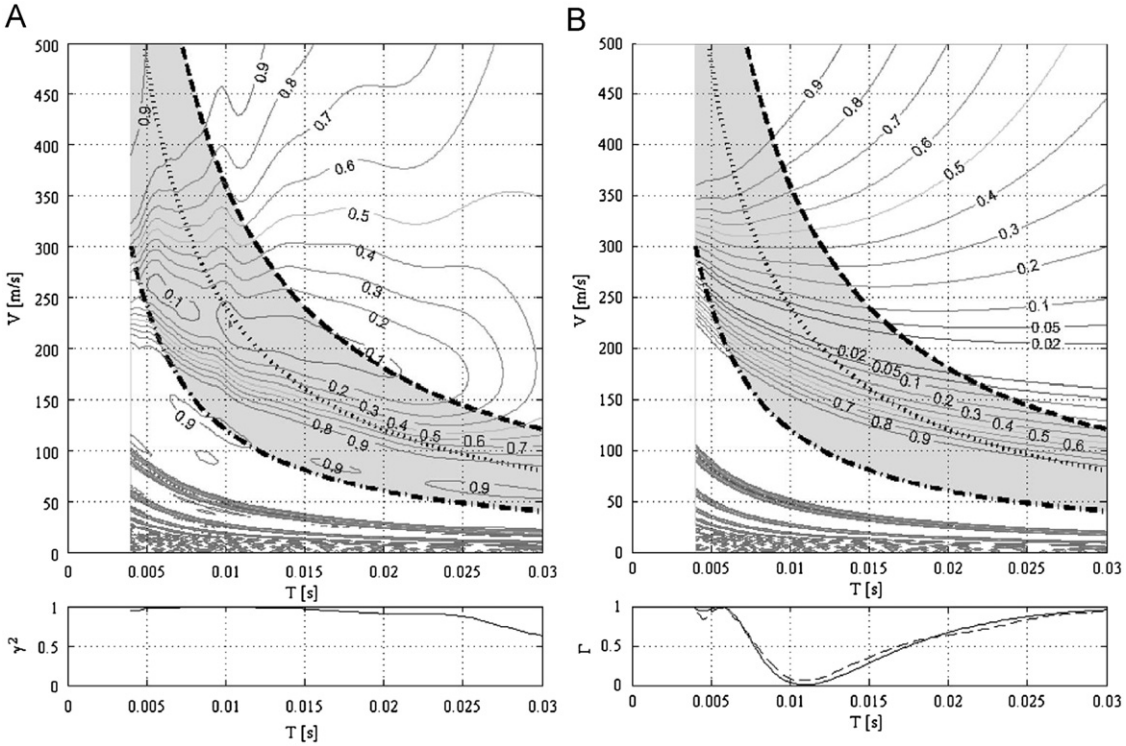

Fig. 14. Spatial phase dispersion for a transducer offset of 0.60 m: (A) Experimental and (B) Analytical.

Table 3
Fitted shear waves velocities for Case 2.

Layer	Thickness (m)	Poisson's ratio	Density (tn/m^3)	V_S (m/s)
1	0.05	1/3	2.30	831
2	0.10	1/3	1.90	422
3	0.20	1/3	1.40	336
4	0.40	1/3	1.40	191
5	0.80	1/3	1.40	200
Halfspace	∞	1/3	1.40	179

Table 3 shows the discretization of the site profile, the adopted values of Poisson's ratio and density, and the final adjusted values of the shear wave velocities. The adjusted velocity of asphalt is consistent with the range of values $V_S = 800-950\,\mathrm{m/s}$ obtained in direct measurements over core samples. The adjusted velocity of the base is found within the expected values. The shear wave velocity for the loess stratum of 0.20 m thickness turns out to be higher than lower strata, which is attributed to surface compaction of the top soil layer. The remaining velocities in loess are found consistent with those at nearby areas measured with other techniques referred to in Case 1.

6. Conclusions

A new technique for adjustment of mechanical soil profiles through the spectral analysis of surface waves has been presented. This technique, based on the complete solution of the response of the ground surface, does not have the limitation of the original SASW method that is rigorously applicable only for soil profiles with growing stiffness in depth. The spatial phase dispersion used as a target function for the adjustment process takes into account the variability of the propagation velocities with the number and the offset of the transducers used in the experimental setup.

A new version of the stiffness matrix of the homogeneous halfspace was derived by means of experimental modal analysis techniques, allowing to use the thin layers formulation to obtain the response in spatial domain in closed form through system modal parameters. In this way the explicit application of Hankel transform is avoided, thus substantially reducing the computational time.

The tests cases have shown the distortions on the experimental phase dispersion produced both by experimental noise and by variations within the layers of the soil profile. The target function for the model adjustment is shown to be robust even in low coherence ranges and with relatively small number of transducers. Further testing of the proposed technique in more complex soil sites and comparison against other techniques may be found useful to assess its reliability for practical applications. Another issue still pending to be addressed in detail is the estimation of uncertainties of the adjusted parameters of the soil profile.

Acknowledgements

The present work was partially supported by the National Research Council of Argentina (CONICET) and the Science and Technology Agency of the Province of Cordoba, Argentina. The writers would like to thank to A. Prato and F. Figueroa for their assistance in carrying out the tests.

Appendix A

The following halfspace matrices with the format of Eq. (1) produce the curves of Fig. 2:

$$A = \begin{bmatrix} A_{11} & A_{21}^T \\ A_{21} & I \end{bmatrix}, \tag{29}$$

$$A_{11} = \begin{bmatrix} 4.604+0.261i & 0 \\ 0 & 0.453+0.027i \end{bmatrix}, \tag{30}$$

$$A_{21} = \begin{bmatrix} 0.230-0.012i & 0 \\ 0 & 0.456-0.319i \\ 1.839+0.086i & 0 \\ 0 & 0.013-0.310i \\ -0.825+0.036i & 0 \\ 0 & 0.448+0.507i \\ 0.242+0.089i & 0 \\ 0 & 0.282-0.082i \end{bmatrix}, \tag{31}$$

$$B = \begin{bmatrix} B_{11} & B_{21}^T \\ B_{21} & B_{22} \end{bmatrix}, \tag{32}$$

$$B_{11} = \begin{bmatrix} 0 & 0.483-0.328i \\ 0.483-0.328i & 0 \end{bmatrix}, \tag{33}$$

$$B_{21} = \begin{bmatrix} 0 & -0226+1.353i \\ 0.394-0.718i & 0 \\ 0 & 0.791-0.218i \\ -0.646-0.457i & 0 \\ 0 & 0.090+0.159i \\ 0.056-0.458i & 0 \\ 0 & 0.242-0.012i \\ -0.437-0.102i & 0 \end{bmatrix}, \tag{34}$$

$$B_{22} = \begin{bmatrix} 0 & -0.816-0.134i & \cdots \\ -0.816-0.134i & 0 & \cdots \\ 0 & 0.177+0.043i & \cdots \\ -0.511-0.080i & 0 & \cdots \\ 0 & -0.239+0.054i & \cdots \\ 0.216-0.209i & 0 & \cdots \\ 0 & 0.075-0.276i & \cdots \\ -0.116-0.174i & 0 & \cdots \end{bmatrix}$$

$$\begin{matrix} \cdots & 0 & -0.511-0.080i & \cdots \\ \cdots & 0.177+0.043i & 0 & \cdots \\ \cdots & 0 & -0.269-0.012i & \cdots \\ \cdots & -0.269-0.012i & 0 & \cdots \\ \cdots & 0 & -0.025+0.112i & \cdots \\ \cdots & 0.070-0.294i & 0 & \cdots \\ \cdots & 0 & 0.231-0.165i & \cdots \\ \cdots & -0.208-0.044i & 0 & \cdots \end{matrix}$$

$$\begin{matrix} \cdots & 0 & 0.216-0.209i & \cdots \\ \cdots & -0.239+0.054i & 0 & \cdots \\ \cdots & 0 & 0.070-0.294i & \cdots \\ \cdots & -0.025+0.112i & 0 & \cdots \\ \cdots & 0 & 0.234+0.030i & \cdots \\ \cdots & 0.234+0.030i & 0 & \cdots \\ \cdots & 0 & 0.133+0.075i & \cdots \\ \cdots & -0.072-0.042i & 0 & \cdots \end{matrix}$$

$$\begin{bmatrix} \cdots & 0 & -0.116-0.174i \\ \cdots & 0.075-0.276i & 0 \\ \cdots & 0 & -0.208-0.044i \\ \cdots & 0.231-0.165i & 0 \\ \cdots & 0 & -0.072-0.042i \\ \cdots & 0.133+0.075i & 0 \\ \cdots & 0 & -0.276+0.023i \\ \cdots & -0.276+0.023i & 0 \end{bmatrix}, \tag{35}$$

$$C = \begin{bmatrix} C_{11} & C_{21}^T \\ C_{21} & C_{22} \end{bmatrix}, \tag{36}$$

$$C_{11} = \begin{bmatrix} -0.631+1.099i & 0 \\ 0 & 0.546-0.359i \end{bmatrix}, \tag{37}$$

$$C_{21} = \begin{bmatrix} 0.213+0.245i & 0 \\ 0 & 0.531-0.832i \\ -0.198+0.330i & 0 \\ 0 & -0.452-0.278i \\ 0.124-0.251i & 0 \\ 0 & -0.253-0.376i \\ -0.177-0.092i & 0 \\ 0 & -0.578-0.068i \end{bmatrix}, \tag{38}$$

$$C_{22} = \mathrm{diag}\begin{bmatrix} 1.574+0.931i \\ 0.388-0.544i \\ 0.137+0.162i \\ -0.402+0.290i \\ -0.325+0.113i \\ -1.037+0.264i \\ -0.481-0.005i \\ -0.927-0.022i \end{bmatrix}. \tag{39}$$

The degrees of freedom 3–10 represent "generalized" (non-physical) coordinates used to extend the modal model to improve the approximation of the flexibility curves.

References

[1] Stokoe II KH, Wright SG, Bay JA, Roesset JM. Characterization of geotechnical sites by SASW Method. In: XIII ICSMFE, New Delhi, India, 1994. p. 15–25.

[2] Lai CG, Rix GJ, Foti S, Roma V. Simultaneous measurement and inversion of surface wave dispersion and attenuation curves. Soil Dynamics and Earthquake Engineering 2002;22:923–30.

[3] Tokimatsu K, Tamura S, Kojima H. Effects of multiple modes on Rayleigh wave dispersion characteristics. Journal of Geotechnical Engineering (ASCE) 1992;118(10):1529–43.

[4] Lin CP, Chang TS. Multi-station analysis of surface wave dispersion. Soil Dynamics and Earthquake Engineering 2004;24:877–86.

[5] Muract J, Suárez LE. Automatización del Método de Análisis Espectral de Ondas Superficiales. In: Proceedings of Sinergia, National University of Córdoba, Argentina, 2004 [in Spanish].

[6] Zywicki DJ. Advanced signal processing methods applied to engineering analysis of seismic surface waves. PhD dissertation, Georgia Institute of Technology, Atlanta; 1999.

[7] Zomorodian SMA, Hunaidi O. Inversion of SASW dispersion curves based on maximum flexibility coefficients in the wave number domain. Soil Dynamics and Earthquake Engineering 2006;26:735–52.

[8] Park CB, Miller RD, Xia J. Multichannel analysis of surface waves. Geophysics 1999;64(3):800–8.

[9] Yoon S. Array-based measurements of surface wave dispersion and attenuation using frequency-wavenumber analysis. PhD dissertation, Georgia Institute of Technology, Atlanta; 2005.

[10] Foti S. Multistation methods for geotechnical characterization using surface waves. PhD dissertation, Politecnico di Torino, Italy; 2000.

[11] Roma V. Soil properties and site characterization by means of Rayleigh waves. PhD dissertation, Politecnico di Torino, Italy; 2001.

[12] Zhang SX, Chan LS, Chen CY, Dai FC, Shen XK, Zhong H. Apparent phase velocities and fundamental-mode phase velocities of Rayleigh waves. Soil Dynamics and Earthquake Engineering 2003;23:563–9.

[13] Strobbia C. Surface wave methods: acquisition, processing and inversion. PhD dissertation, Politecnico di Torino, Italy; 2002.

[14] Xia J, Miller RD, Park CB, Tian G. Inversion of high frequency surface waves with fundamental and higher modes. Journal of Applied Geophysics 2003;52:45–57.

[15] Ganji V, Gucunski N, Nazarian S. Automated inversion procedure for spectral analysis of surface waves. Journal of Geotechnical and Geoenvironmental Engineering (ASCE) 1998;124(8):757–70.

[16] Ryden N, Park CB, Ulriksen P, Miller RD. Multimodal approach to seismic pavement testing. Journal of Geotechnical and Geoenvironmental Engineering (ASCE) 2004;130(6):636–45.

[17] Ryden N, Park CB. Fast simulated annealing inversion of surface waves on pavement using phase-velocity spectra. Geophysics 2006;71(4):R49–58.

[18] Park CB, Miller RD, Xia J. Multimodal analysis of high frequency surface waves. In: Proceedings of SAGEEP, Oakland, California, 1999.

[19] Park CB, Miller RD, Xia J. Offset and resolution of dispersion curve in multichannel analysis of surface waves (MASW). In: Proceedings of SAGEEP, Denver, Colorado, 2001.

[20] Kausel E. An explicit solution for the Green functions for dynamic loads in layered media. MIT Research Report R81-13, Department of Civil Engineering, Cambridge; 1981.

[21] Kausel E, Roesset JM. Stiffness matrices for layered soils. Bulletin of the Seismological Society of America 1981;71(6):1743–61.

[22] Ceballos MA, Car EJ, Prato TA, Prato CA, Alvarez LM. Experimental and numerical determination of the dynamic properties of the reactor building of Atucha II NPP. Nuclear Engineering and Design 1998;182: 93–106.

[23] Degrande G, Badsar SA, Lombaert G, Schevenels M, Teughels A. Application of the coupled local minimizers method to the optimization problem in the Spectral Analysis of Surface Waves method. Journal of Geotechnical and Geoenvvironmental Engineering (ASCE) 2008;134(10):1541–53.

[24] Kausel E. Fundamental solutions in elastodynamics: a compendium. New York: Cambridge University Press; 2006.

[25] Maia NMM, Silva JMM, editors. Theoretical and experimental modal analysis. England: Research Studies Press Ltd.; 1997.

[26] Wolf JP. Foundation vibration analysis using simple physical models. New Jersey: PTR Prentice-Hall Inc; 1994.

[27] Ceballos MA, Prato CA. Modal description of foundation dynamics. In: XX international modal analysis conference, Los Angeles, CA, 2002.

[28] Ceballos MA. Análisis modal experimental aplicado a la calibración de modelos de sistemas con interacción suelo-estructura. PhD dissertation, National University of Cordoba, Argentina; 2004 [in Spanish].

[29] Garvey SD, Penny JET, Friswell MI. The relationship between the real and imaginary parts of complex modes. Journal of Sound and Vibration 1998;212(1):75–83.

[30] Garvey SD, Friswell MI, Penny JET. Some further insight into self-adjoint second-order systems. Journal of Vibration and Control 1999;5:237–52.

[31] Lamb H. On the propagation of tremors over the surface of an elastic solid. Philosophical Transactions of the Royal Society of London 1904;A203: 1–42.

[32] Friswell MI, Adhikari S. Derivatives of complex eigenvectors using Nelson's method. AIAA Journal 2000;37(12):2355–7.

[33] Clariá JJ, Rinaldi VA. Relación de Poisson medida en loess inalterado por medio de análisis multimodal. In: XVII Congreso Argentino de Mecánica de Suelos e Ingeniería en Fundaciones, Cordoba, Argentina; 2004 [in Spanish].

[34] Rinaldi VA, Clariá JJ, Santamarina JC. The small-strain shear modulus (Gmax) of argentinean loess. In: XV international conference on soil mechanics and geotechnical engineering, Istanbul, Turkey, vol. 1. 2001. p. 495–9.

[35] Rinaldi VA, Redolfi ER, Santamarina JC. Characterization of collapsible soils with combined geophysical and penetration testing. In: Robertson PK, Mayne PW, editors. Geotechnical site characterization, vol. 1. Rotterdam: Balkema; 1998. p. 581–8.